Clinical and Translational Radiation Oncology 7 (2017) 13–19

Contents lists available at ScienceDirect

Clinical and Translational Radiation Oncology

journal homepage: www.elsevier.com/locate/ctro

Original Research Article

# Prospective analysis of in vivo landmark point-based MRI geometric distortion in head and neck cancer patients scanned in immobilized radiation treatment position: Results of a prospective quality assurance protocol

Joint Head and Neck Radiotherapy-MRI Development Cooperative
Contributing authors: Abdallah S.R. Mohamed [a,d], Chase Hansen [a], Joseph Weygand [b], Yao Ding [a,c], Stephen J. Frank [a], David I. Rosenthal [a], Ken-Pin Hwang [c], John D. Hazle [c], Clifton D. Fuller [c,*], Jihong Wang [b,*]

[a] Department of Radiation Oncology, The University of Texas MD Anderson Cancer Center, Houston, TX, USA
[d] Department of Clinical Oncology and Nuclear Medicine, Faculty of Medicine, University of Alexandria, Alexandria, Egypt
[b] Department of Radiation Physics, The University of Texas MD Anderson Cancer Center, Houston, TX, USA
[c] Department of Imaging Physics, The University of Texas MD Anderson Cancer Center, Houston, TX, USA

ARTICLE INFO

*Article history:*
Received 9 August 2017
Revised 9 September 2017
Accepted 11 September 2017
Available online 10 October 2017

*Keywords:*
MRI
CT
Geometric Distortion
Head and Neck Cancer
Radiation Treatment
Quality Assurance

ABSTRACT

*Purpose:* Uncertainties related to geometric distortion are a major obstacle for effectively utilizing MRI in radiation oncology. We aim to quantify the geometric distortion in patient images by comparing their in-treatment position MRIs with the corresponding planning CTs, using CT as the non-distorted gold standard.

*Methods:* Twenty-one head and neck cancer patients were imaged with MRI as part of a prospective Institutional Review Board approved study. MR images were acquired with a T2 SE sequence ($0.5 \times 0.5 \times 2.5$ mm voxel size) in the same immobilization position as in the CTs. MRI to CT rigid registration was then done and geometric distortion comparison was assessed by measuring the corresponding anatomical landmarks on both the MRI and the CT images. Several landmark measurements were obtained including; skin to skin (STS), bone to bone, and soft tissue to soft tissue at specific levels in horizontal and vertical planes of both scans. Inter-observer variability was assessed and interclass correlation (ICC) was calculated.

*Results:* A total of 430 landmark measurements were obtained. The median distortion for all landmarks in all scans was 1.06 mm (IQR 0.6–1.98). For each patient 48% of the measurements were done in the right-left direction and 52% were done in the anteroposterior direction. The measured geometric distortion was not statistically different in the right-left direction compared to the anteroposterior direction ($1.5 \pm 1.6$ vs. $1.6 \pm 1.7$ mm, respectively, $p = 0.4$). The magnitude of distortion was higher in the STS peripheral landmarks compared to the more central landmarks ($2.0 \pm 1.9$ vs. $1.2 \pm 1.3$ mm, $p < 0.0001$). The mean distortion measured by observer one was not significantly different compared to observer 2, 3, and 4 (1.05, 1.23, 1.06 and 1.05 mm, respectively, $p = 0.4$) with ICC = 0.84.

*Conclusion:* MRI geometric distortions were quantified in radiotherapy planning applications with a clinically insignificant error of less than 2 mm compared to the gold standard CT.



* Corresponding authors at: Head and Neck Section, Division of Radiation Oncology, Department of Radiation Oncology, The University of Texas MD Anderson Cancer Center, Box 0097, 1515 Holcombe Blvd., Houston, TX 77030, USA (C.D. Fuller). Department of Radiation Physics, The University of Texas MD Anderson Cancer Center, 1515 Holcombe Blvd., Houston, TX 77030, USA (J. Wang).

*E-mail addresses:* cdfuller@mdanderson.org (C.D. Fuller), Jihong.Wang@mdanderson.org (J. Wang).

https://doi.org/10.1016/j.ctro.2017.09.003

## Introduction

There has been a steady increase in the utilization of magnetic resonance imaging (MRI) in radiation therapy (RT) for treatment planning because of its superior soft tissue contrast, including tumor conspicuity. Recent advancements in integrated MRI guided radiation therapy systems further enable the tracking of patient's gross tumor volume (GTV) and other critical organs in real-time during treatment [1–3]. This significant technical improvement promises increasing accuracy and fidelity of the actual dose delivered. However, MRI can have larger geometric distortions than X-ray computed tomography (CT), resulting from the scanner's magnetic field imperfections ($B_0$ inhomogeneity and gradient nonlinearity) [4–8], and patient-related effects such as susceptibility variations between different tissues [9,10]. To be used as a primary RT planning modality, MRI's geometric distortion must be compensated by increasing margins after target delineation, resulting in limited capacity for dose reduction to the surrounding normal tissues.

At present, CT remains the imaging modality of choice for treatment planning and the gold standard for GTV delineation and adaptive RT applications. Compared with MRI, CT has minimal geometric distortion and its intrinsic information on electron density for dose calculation of various tissues, making it a natural imaging choice for treatment planning [11]. In head and neck cancer (HNC), CT provides better visualization of cortical bone invasion and tumor-fat boundaries than MRIs. However, poor soft tissue contrast, which is extremely critical in determining tumor edges, organs at risk, and bone marrow, remains a major limitation for CT utilization as a single image modality in RT applications [7]. Additionally, CT is susceptible to metal artifacts caused by dental fillings and other prosthesis. These limitations require the additional use of other imaging modalities, like MRI or positron emission tomography (PET), which complement each other to allow for precise target definition and organ at risk sparing.

As a part of an on-going research effort aiming to develop MR-guided RT platforms, we have been acquiring MR images of HNC patients in their customized radiation immobilization devices, to match their radiation therapy treatment position, as well as their CT treatment scanning position [12]. In this study, we aim to quantify the geometric distortion in patient images by comparing their in-treatment position MRIs with the corresponding planning CTs, using CT as the non-distorted gold standard.

Our specific aims are to (1) determine the intra- and inter-observer variation that exists when measuring specific distances between landmarks on both CT and MR images after rigid co-registration, and (2) verify that MRI geometric distortion is within practical limits to support increased clinical utility of MRI guided radiotherapy, particularly for future MRI-only treatment planning and the combined MR-CT systems.

## Materials and methods

### *Patient selection*

As part of a programmatic effort to develop quality assurance and performance tolerance for MRI-guided radiotherapy, twenty-one HNC patients were selected in this prospective study, after obtaining institutional review board approval and written informed consents from all participants. Criteria of patient's inclusion were; age $\geq$18 years, histologically documented stage III or IV human papillomavirus positive (HPV+) squamous cell carcinoma of the oropharynx, definitive chemoradiotherapy, Eastern Cooperative Oncology Group (ECOG) performance status of 0–2, and no contraindications to MRI. All patients had their treatment planning CT done within one week of the MRI to avoid any significant anatomical changes between both images (e.g. tumor progression or weight loss). Both images were collected prior to the initiation of treatment.

### *Imaging acquisition*

#### *MRI*

MR images were acquired with a 3.0-T Discovery 750 MRI scanner (GE Healthcare, Waukesha, WI, USA) with laterally placed 6-channel phased array flex coils (GE Healthcare) centered on tumor covering from palatine process down to the lower edge of cricoid cartilage. T2-weighted fast spin echo (FSE) sequence were acquired in the same immobilization position as in the treatment planning CT scans as described in details in a previous report [12]. By doing so, we minimized patient positioning differences in the acquisition of CT and MR images resulting in a minimized registration error between the two sets of images. Specific imaging acquisition parameters of the T2-weighted FSE sequence are as follows: FOV = 256 mm, Slice thickness = 2.5 mm and Matrix = 512 $\times$ 512, giving pixel size of 0.5 $\times$ 0.5 $\times$ 2.5 mm; Repetition Time (TR) = 3.7 s; Echo Time (TE) = 97 ms; Echo Train Length (ETL) = 16. The distance from the skin surface to the center of FOV was less than 10 cm for all patients included in this study.

#### *CT*

CT was acquired using the standard institutional protocol for simulation non-contrast enhanced CT; slice thickness = 2.5 mm, tube current = 350 mA at 120 kVp, display field of view = 500 mm, matrix of 512 $\times$ 512 pixels, pixel size of 0.98 $\times$ 0.98 mm, isocenter at arytenoid cartilage, and coverage from vertex to carina.

### *Image selection and evaluation of geometric distortion*

CT and T2-weighted MRI were transferred to commercial image registration and segmentation software VelocityAI (Velocity Medical Solutions, Atlanta, GA). The navigator module was selected, and the T2 MRI was rigidly registered to the CT. The module consists of selection of primary (CT) and secondary (T2 MRI) images, manual alignment, selection of region of interest, and rigid registration. Deformable registration was not used in order to assess the inherent distortion in MRI.

Utilizing the measurement tool within the VelocityAI software, several skin to skin (STS, total of 9 landmarks), bone to bone (BTB, 9 landmarks), and soft tissue to soft tissue (TTT, 3 landmarks) measurements were done at specific levels in horizontal and vertical direction of both CT and MRI images. Landmarks were anatomical features that can be reliably identified and reproduced by observers on both CT and MRI. Table 1 illustrates the details of the anatomical boundaries of the selected landmarks. The difference between measurements of corresponding anatomical landmark on both MR and CT images was considered to be overall geometric distortion. Fig. 1 summarizes the workflow process utilized to obtain these measurements.

The landmarks were mainly selected in three levels (i.e. upper, middle, and lower). Criteria for selecting each of the three specific imaging levels were as follows: the top slice was the cranial-most co-registered image depicting clear maxillary sinuses and homogenous intensity. Clear lower edge of the mandible, anterior vertebral body, and complete vertebral encasing of the vertebral canal distinguished the middle slice. Similarly, the caudal-most image was selected based on clear superior border of the body of hyoid bone, anterior vertebral body, and complete vertebral encasing of the vertebral canal. Nearly 43% of the anatomical landmarks are peripheral (skin to skin) while the rest are more central landmarks such as two points on a bony structure or muscle structures as

**Table 1**
List of the selected landmarks.

*Skin to skin landmarks*
1. Horizontal line at the level of pterygomaxillary fissure
2. Horizontal line at level of tip of lateral pterygoid plate
3. Horizontal line at level of the pterygoid notch
4. Oblique line passing through the left zygomatic process and pharyngeal tubercle at midline
5. Vertical line passing through the left zygomatic process and the lateral edge of left cerebellar tonsil.
6. Vertical midline at the level of superior border of body of hyoid bone
7. Horizontal line at the level of anterior vertebral body of the inferior border of C2
8. Horizontal line at the level of anterior vertebral body of the inferior border of C4
9. Vertical midline at the level of inferior border of C4

*Bone to bone landmarks*
1. Horizontal line between the medial edge of bilateral mandibular condyles
2. Horizontal line between the tip of bilateral mastoid processes
3. Vertical line between the mentum and the midpoint of the anterior surface of the vertebral body
4. Vertical midline of the spinal canal of C2
5. Horizontal line of the spinal canal of C2
6. Horizontal line between the angles of the mandible
7. Vertical midline of the spinal canal of C4
8. Horizontal line of the spinal canal of C4
9. Vertical line between the midpoint of the posterior border of the superior surface of body of hyoid bone to the midpoint of anterior vertebral body

*Soft tissue to soft tissue landmarks*
1. Right lateral pterygoid muscle vertical length
2. Vertical midline cerebellar length
3. Left sternocleidomastoid muscle vertical width

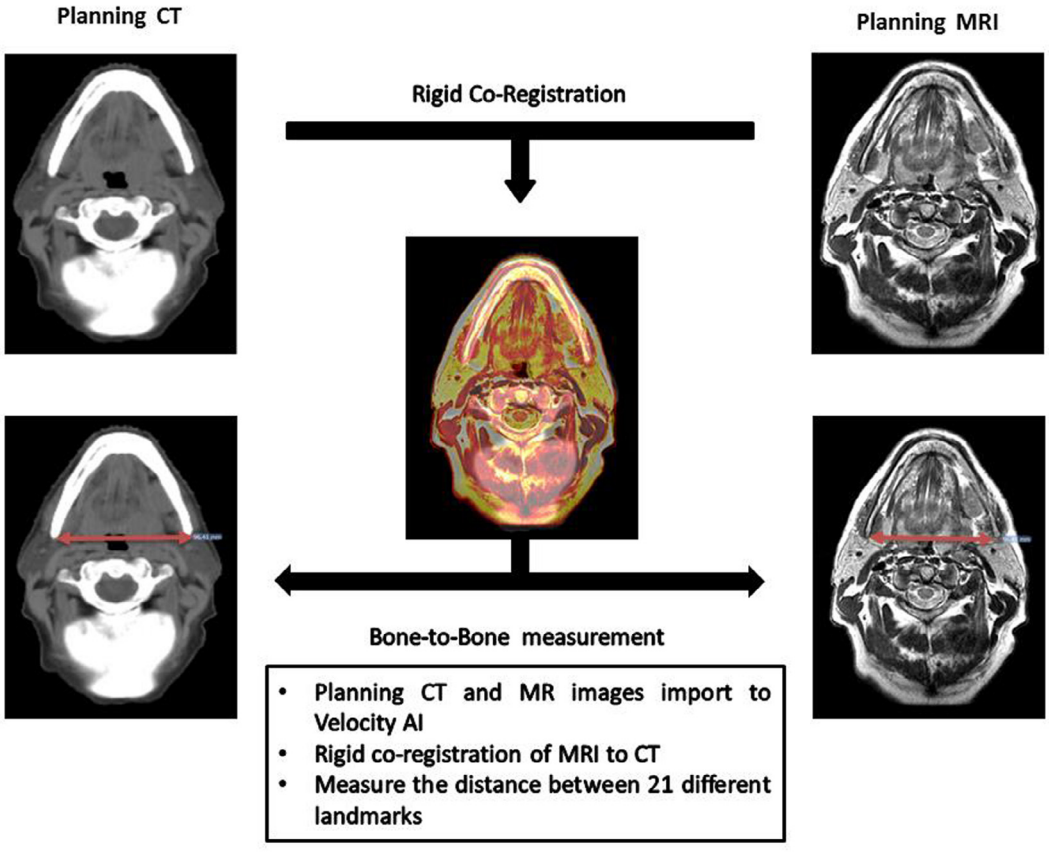


**Fig. 1.** This figure depicts the workflow of anatomical landmark measurements and comparison.

illustrated in Table 1. For each patient, ten (48%) of the measurements were distances in the horizontal direction while the rest were in the anteroposterior direction. Also the landmarks were chosen to be distributed in the upper, middle and lower sections of the head and neck (Fig. 2). Geometric error was subsequently compared for all different axes, levels, and nature.

*Inter- and intra-observer variation*

For assessment of intra-observer variation, a single observer repeated a total of 100 landmark measurements (i.e. 10 landmark measurements per patient for 10 patients) to determine the intra-observer variation. For assessment of inter-observer variation in

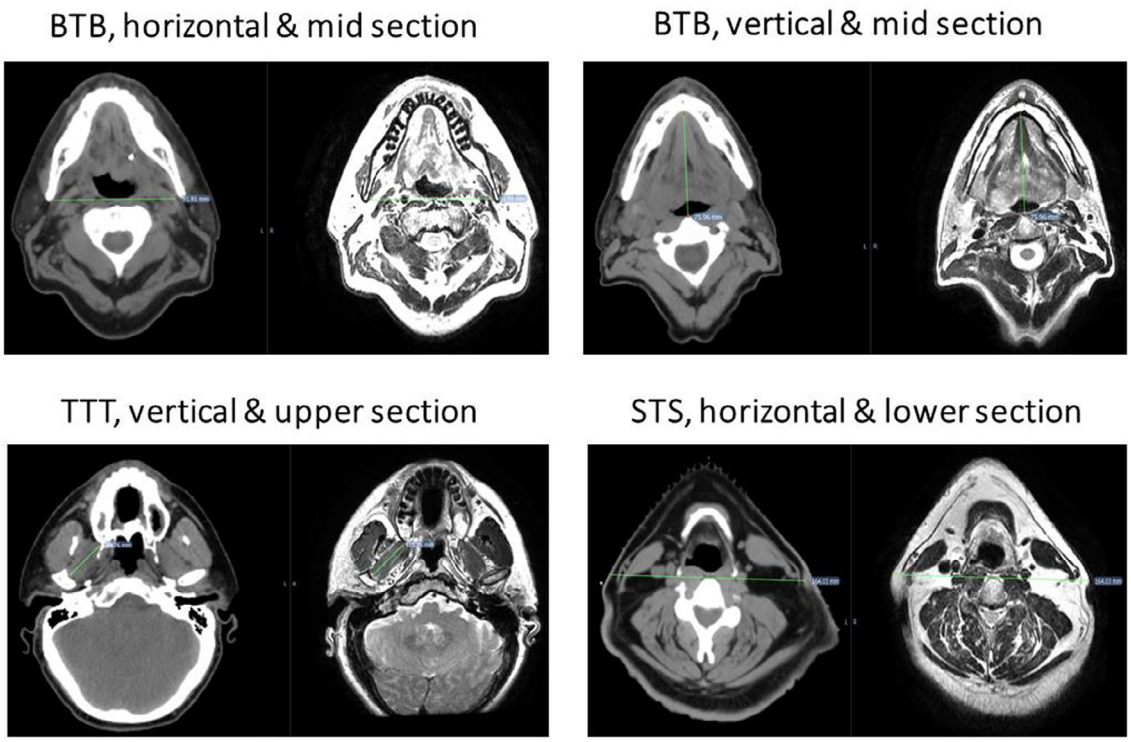


**Fig. 2.** Examples of anatomical landmarks included in the study. These landmarks were strategically selected to encompass a broad coverage of the anatomical areas and varieties of anatomical structures (bone, soft tissue) and direction (vertical vs. horizontal).

landmark measurement, four observers collectively repeated the assigned 100 measurements independently to assess the inter-observer variation.

*Statistical analysis*

Numeric variables are expressed in mean and SD. Comparison of mean errors by different stratification was done using non parametric statistics, $p < 0.05$ was considered statistically significant.

Intraclass correlation (ICC) was calculated for intra- and inter-observer variation. All analyses were done with JMP v 11Pro (SAS institute, Cary, NC), and Microsoft Excel (Redman, Washington).

## Results

*Geometric distortion*

Eleven landmark points were not attainable due to variation in the range of MR coverage in four patients' scans, leaving a total of 430 landmark measurements for final analysis. The mean distortion for all landmark measurements in all scans was 1.6 ± 1.7 mm. There were no statistically significant difference of distortion magnitude for measurements at the horizontal vs. vertical direction (1.5 ± 1.6 vs. 1.6 ± 1.7 mm, respectively, $p = 0.4$) as shown in Fig. 3. Likewise, there were no significant differences in error measurements in the upper, middle, and lower section of the head and neck (1.5 ± 1.6 vs. 1.4 ± 1.2 vs. 1.7 ± 1.9 mm, respectively, $p = 0.3$) as shown in Fig. 4. However, we observed a statistically significant difference in peripheral (STS) vs. more central landmarks (2.0 ± 1.9 vs. 1.2 ± 1.3 mm, respectively, $p < 0.0001$) as shown in Fig. 5.

*Inter- and intra-observer variations*

The average error measurements between the MRI and respective CT for the selected 100 landmarks were 1.05 ± 0.87, 1.23 ± 0.82, 1.06 ± 0.99 and 1.05 ± 0.79 mm for observer 1, 2, 3, and 4, respectively as shown in Supplementary Fig. 1. The ICC for inter-observer variation was 0.84 (95% CI, 0.78–0.88). Likewise, the average error for repeated measurements of observer 1 were 0.97 mm for the initial measurement and 0.99 mm for the repeats ($p = 0.9$) and the ICC for intra-observer variation was 0.76 (95% CI, 0.64–0.84).

## Discussion

Our results showed that the overall average discrepancies of geometric fidelity of MRI were within 2 mm from that of the CT. We also demonstrated that there were no significant differences in the degree of geometric distortion in different axes and levels of the studied MR images. However, distortions were significantly higher peripherally for skin to skin landmarks than for more central bone to bone of soft tissue to soft tissue landmarks. These results were consistent among different observer and with repeated measurements for the same single observer with excellent ICC for both inter- and intra-observer observations.

One of the main goals of radiotherapy is to accurately define the tumor target with high certainty. MRI has superior soft tissue contrast enabling better delineation of tumor from those of surrounding healthy tissues, where the relatively poor contrast of CT resulted in uncertainties in target delineation. Therefore, in spite of the fact that MRI has a certain degree of distortion, MRI may still provide higher confidence in target delineation and consistency compared with CT. Our data support that additional margins around target volumes to account for geometric uncertainty may not be needed for radiotherapy planning using anatomical MR sequences particularly if tumors are close to the image isocenter. This is partly because the relatively small error introduced by geometric distortion compared with higher inter-observer delineation error observed in radiotherapy planning using CT, as widely published in the literature [13–15]. We are also running a separate investigation of the inter-observer delineation error using

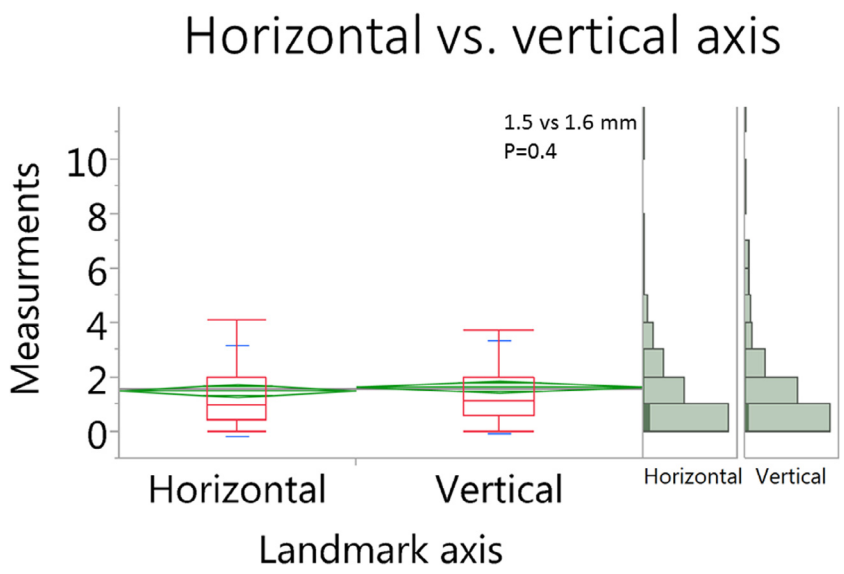


**Fig. 3.** Box plots for the landmark measurements in horizontal vs. vertical axis.

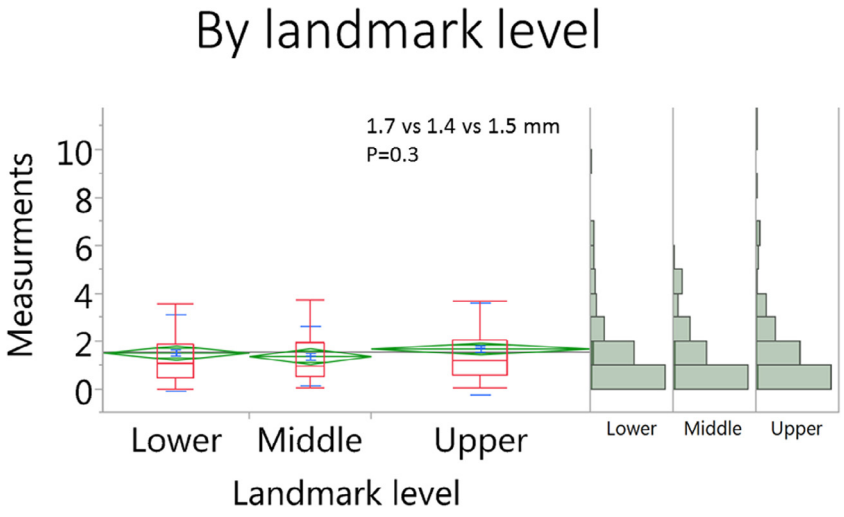


**Fig. 4.** Box plots for the landmark measurements in the upper, middle, and lower section of the head and neck.

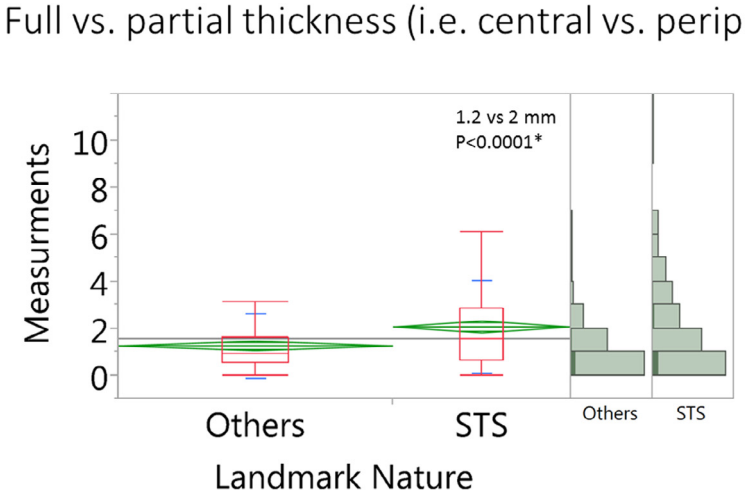


**Fig. 5.** Box plots for the landmark measurements in the peripheral vs. central landmarks.

anatomical MR sequences acquired using the radiotherapy immobilization platform used in the current study. However, for functional MR sequences (e.g. diffusion weighted imaging) the magnitude of distortion is much higher and requires dedicated study to investigate its optimal use in radiotherapy planning context [16,17].

Geometric distortion due to MRI scanner system imperfection is also spatially dependent. The magnitude of distortion is typically small at isocenter (the center of the magnet and gradient system) and larger in areas away from isocenter (i.e. near the skin) due to the falloff in gradient linearity at the periphery. Therefore, the actual geometric distortion in practice can be smaller than the average distortion reported in this study, depending on the tumor and other structure location. For head and neck cancer patients, the region of MR imaging volume is relatively small and can be completely contained by the "sweet zone" (i.e. area of relatively linear gradients and homogeneous B0 field). For other anatomical areas such as the GI and GU, and when the tumor is off to the peripheral of the body, the geometric distortion may be larger than that of the central location. Thus, the geometric distortion for those specific anatomical areas may still need to be assessed for radiation therapy applications. Additionally, each MRI scanner system's geometric distortion is different and, thus, must be assessed individually.

Susceptibility-induced geometric inaccuracies occur at boundaries between tissues with large differences in susceptibility (e.g. bone-tissue, air cavity-tissues). Those geometric inaccuracies are difficult to assess but usually occur in the frequency encoding direction and can be somewhat minimized by increasing the bandwidth in the MRI acquisition. From the results of our measurements, the overall discrepancies (which include the susceptibility induced inaccuracies, system-specific inaccuracies, and the registration error between CT and MR) are within 2 mm, which is an encouraging finding.

Additionally, MRI is more complicated than CT in which many acquisition parameters may affect the geometric distortion. Therefore, for each clinical practice, the commonly used MRI acquisition sequences and parameters need to be optimized based on the recommendations of physicists or vendors. The actual distortion must be assessed by phantoms, and quality control program needs to be in place to ensure such consistency and quality.

At the present, there is no specific, commonly agreed upon guidelines for the quality control and quality assessment for MRI geometric distortion. Professional organization such as the AAPM has established several task groups (e.g. AAPM TG117) looking into these very issues. There is lack of commonly agreeable phantom to use in the assessment of geometric fidelity. For radiotherapy applications, minimizing geometric distortion is a fundamental element before clinical implementation. Several prior attempts were implemented to optimize the MR sequences, including using 3D spin echo sequences with vendor-supplied distortion correction and widening the bandwidth to reduce susceptibility related distortion [18,19]. Placement of the region of interest at or near the isocenter of the magnet, where gradient field nonlinearities are minimum is another solution. Additionally, increasing the sampling bandwidth at the cost of SNR, because the bandwidth is inversely proportional to susceptibility-induced errors is another alternative for radiotherapy applications where very high SNR may not be as critical as in diagnostic applications.

Our study is limited by the relatively small number of patients in the study. However, this is our attempt to measure the actual discrepancies in geometric fidelity as compared with CT, which is considered to have little or no distortion. This study is still valid because the large number of landmark measurements included. Furthermore, the MRI sequence (T2w) we used in this study was a multiple 2D acquisition with a slice thickness of 2.5 mm (superior-inferior direction) which, thereby, has lower resolution compared with the in-plane (anterior-posterior and right-left) that was 0.5 mm. Therefore, reliable and reproducible landmarks in the superior-inferior direction were not attainable. While for slice locations away from the isocenter, the axial planes tend to "warp", introducing out-of-plane distortion. This introduces additional uncertainties in geometric fidelity in MRI. Therefore, it is critical to apply 3D geometric distortion correction in the acquisition to minimize the out-of-plane distortion. Also, our study did not explore the possibilities of further optimizing the pulse sequences in the image acquisition such that distortion due to MRI can be further minimized, and the scanner used in our study is a regular MRI scanner used for diagnostic purpose, rather than optimized for radiation therapy treatment planning purposes. It is expected that with MRI scanners that are designed for such purpose, the geometric distortion and optimization of MRI sequences, the distortion due to MRI can be reduced further.

Our future works include the assessment of geometric discrepancies between CT simulation scans and that of MRI in other anatomical areas such as GI and GU. These other studies present other challenges including patient and internal organ motion and the needs of developing patient immobilization devices and procedures for MRI scans. Despite the challenges, these kinds of validation studies are important and much needed for using MRI in radiotherapy applications. This current study has given us the confidence that the geometric distortion in MRI is manageable and is within a reasonable range. With proper immobilization devices, optimization of MRI sequences, and QA/QC procedure in the future, implementing MRI for radiation therapy treatment planning in most if not all anatomical areas are possible.

## Conflict of interest statement

The authors declare no conflicts of interest.

## Funding sources and financial disclosures

Drs., Mohamed and Fuller receive(d) funding support from the National Institutes of Health (NIH)/National Institute for Dental and Craniofacial Research (1R01DE025248-01/R56DE025248-01). Dr. Fuller received/receives grant and/or salary support from: the NIH/National Cancer Institute (NCI) Head and Neck Specialized Programs of Research Excellence (SPORE) Developmental Research Program Award (P50CA097007-10) and Paul Calabresi Clinical Oncology Program Award (K12 CA088084-06); a National Science Foundation (NSF), Division of Mathematical Sciences, Joint NIH/NSF Initiative on Quantitative Approaches to Biomedical Big Data (QuBBD) Grant (NSF 1557679); the NIH Big Data to Knowledge (BD2K) Program of the National Cancer Institute (NCI) Early Stage Development of Technologies in Biomedical Computing, Informatics, and Big Data Science Award (1R01CA214825-01); NCI Early Phase Clinical Trials in Imaging and Image-Guided Interventions Program (1R01CA218148-01); a General Electric Healthcare/MD Anderson Center for Advanced Biomedical Imaging In-Kind Award; an Elekta AB/MD Anderson Department of Radiation Oncology Seed Grant; the Center for Radiation Oncology Research (CROR) at MD Anderson Cancer Center; and the MD Anderson Institutional Research Grant (IRG) Program. Dr. Fuller has received speaker travel funding from Elekta AB. Supported in part by the National Institutes of Health (NIH)/National Cancer Institute (NCI) Cancer Center Support (Core) Grant CA016672 to The University of Texas MD Anderson Cancer Center. Joe Weygand is partially funded by an Elekta sponsored grant. Jihong Wang is partially funded by a GE-in-kind grant.

## Appendix A. Supplementary data

Supplementary data associated with this article can be found, in the online version, at http://dx.doi.org/10.1016/j.ctro.2017.09.003.

## References


[1] Mutic S, Dempsey JF. The ViewRay system: magnetic resonance-guided and controlled radiotherapy. Semin Radiat Oncol 2014;24:196–9.
[2] Raaymakers BW, de Boer JC, Knox C, Crijns SP, Smit K, Stam MK, et al. Integrated megavoltage portal imaging with a 1.5 T MRI linac. Phys Med Biol 2011;56:N207–14.
[3] Fallone BG, Murray B, Rathee S, Stanescu T, Steciw S, Vidakovic S, et al. First MR images obtained during megavoltage photon irradiation from a prototype integrated linac-MR system. Med Phys 2009;36:2084–8.
[4] Matakos A, Balter J, Cao Y. Estimation of geometrically undistorted B(0) inhomogeneity maps. Phys Med Biol 2014;59:4945–59.
[5] Hong C, Lee DH, Han BS. Characteristics of geometric distortion correction with increasing field-of-view in open-configuration MRI. Magn Reson Imaging 2014;32:786–90.
[6] Aubry JF, Cheung J, Morin O, Beaulieu L, Hsu IC, Pouliot J. Investigation of geometric distortions on magnetic resonance and cone beam computed tomography images used for planning and verification of high-dose rate brachytherapy cervical cancer treatment. Brachytherapy 2010;9:266–73.
[7] Webster GJ, Kilgallon JE, Ho KF, Rowbottom CG, Slevin NJ, Mackay RI. A novel imaging technique for fusion of high-quality immobilised MR images of the head and neck with CT scans for radiotherapy target delineation. Br J Radiol 2009;82:497–503.
[8] Weygand J, Fuller CD, Ibbott GS, Mohamed ASR, Ding Y, Yang J, et al. Spatial precision in magnetic resonance imaging-guided radiation therapy: the role of geometric distortion. Int J Radiat Oncol Biol Phys 2016;95:1304–16.
[9] Stanescu T, Wachowicz K, Jaffray DA. Characterization of tissue magnetic susceptibility-induced distortions for MRIgRT. Med Phys 2012;39:7185–93.
[10] Wang H, Balter J, Cao Y. Patient-induced susceptibility effect on geometric distortion of clinical brain MRI for radiation treatment planning on a 3T scanner. Phys Med Biol 2013;58:465–77.
[11] Jager EA, Kasperts N, Caldas-Magalhaes J, Philippens ME, Pameijer FA, Terhaard CH, et al. GTV delineation in supraglottic laryngeal carcinoma: interobserver agreement of CT versus CT-MR delineation. Radiat Oncol 2015;10:26.
[12] Ding Y, Mohamed ASR, Yang J, Colen RR, Frank SJ, Wang J, et al. Prospective observer and software-based assessment of magnetic resonance imaging quality in head and neck cancer: should standard positioning and immobilization be required for radiation therapy applications? Pract Radiat Oncol 2015;5:e299–308.
[13] Segedin B, Petric P. Uncertainties in target volume delineation in radiotherapy – are they relevant and what can we do about them? Radiol Oncol 2016;50:254–62.
[14] Hong TS, Tome WA, Harari PM. Heterogeneity in head and neck IMRT target design and clinical practice. Radiother Oncol 2012;103:92–8.
[15] Rasch CR, Steenbakkers RJ, Fitton I, Duppen JC, Nowak PJ, Pameijer FA, et al. Decreased 3D observer variation with matched CT-MRI, for target delineation in Nasopharynx cancer. Radiat Oncol 2010;5:21.
[16] Barth BK, Cornelius A, Nanz D, Eberli D, Donati OF. Diffusion-weighted imaging of the prostate: image quality and geometric distortion of readout-segmented versus selective-excitation accelerated acquisitions. Invest Radiol 2015;50:785–91.
[17] Verhappen MH, Pouwels PJ, Ljumanovic R, van der Putten L, Knol DL, De Bree R, et al. Diffusion-weighted MR imaging in head and neck cancer: comparison between half-Fourier acquired single-shot turbo spin-echo and EPI techniques. AJNR Am J Neuroradiol 2012;33:1239–46.
[18] Wang D, Strugnell W, Cowin G, Doddrell DM, Slaughter R. Geometric distortion in clinical MRI systems Part I: evaluation using a 3D phantom. Magn Reson Imaging 2004;22:1211–21.
[19] Port JD, Pomper MG. Quantification and minimization of magnetic susceptibility artifacts on GRE images. J Comput Assist Tomogr 2000;24:958–64.